Journal of Intelligent Manufacturing (2020) 31:1191–1201
https://doi.org/10.1007/s10845-019-01505-9

Towards defect monitoring for metallic additive manufacturing components using phased array ultrasonic testing

A. Chabot[1,2] · **N. Laroche**[3,4] · **E. Carcreff**[4] · **M. Rauch**[1,2] · **J.-Y. Hascoët**[1,2]

Received: 25 March 2019 / Accepted: 15 October 2019 / Published online: 30 October 2019

Abstract

Additive manufacturing (AM) is a rising technology bringing new opportunities for design and cost of manufacturing, compared to standard processes like casting and machining. Among the AM techniques, direct energy deposition (DED) processes are dedicated to manufacture functional metallic parts. Despite of their promising perspectives, the industrial implementation of DED processes is inhibited by the lack of structural health control. Consequently, non-destructive testing (NDT) techniques can be investigated to inspect DED-manufactured parts, in an online or offline manner. To date, most ultrasonic NDT applications to metallic AM concerned the selective laser melting process; existing studies tackling DED processes mainly compare various ultrasonic techniques and do not propose a comprehensive control method for such processes. Current researches in the GeM laboratory focus on a multi-sensor monitoring method dedicated to DED processes, with a structural health control loop included, in order to track defect formation during manufacturing. In this way, this paper aims to be a proof of concept and proposes a comprehensive control method that opens the way to in situ ultrasonic control for DED. In this paper, a control method using the phased array ultrasonic testing (PAUT) technique is particularly illustrated on wire-arc additive manufacturing (WAAM) components, and its applicability to laser metal deposition (LMD) is also demonstrated. A specific attention is given to the calibration method, towards a quantitative prediction of the size of the detected flaws. PAUT predictions are cross-checked thanks to X-ray radiography, which demonstrates that the PAUT method enables to detect and dimension defects from 0.6 to 1 mm for WAAM aluminum alloy parts. Then, an applicable scenario of inspection of a WAAM industrial and large-scale part is presented. Finally, perspectives for in situ and real-time application of the chosen method are given. This paper shows that real-time monitoring of the WAAM process is possible, as the PAUT method can be integrated in the manufacturing environment, provides relevant in situ data, and runs with computing times compatible with real-time applications.

Keywords Additive manufacturing · Direct energy deposition · WAAM · Process control · Phased array ultrasonic testing

Abbreviations

AM	Additive manufacturing
DED	Direct energy deposition
GMAW	Gas-metal arc welding
GPU	Graphic processing unit
LMD	Laser metal deposition
NDT	Non-destructive testing
PAUT	Phased-array ultrasonic testing
PWI	Plane wave imaging
RT	Radiography testing

✉ A. Chabot
alexia.chabot@ec-nantes.fr

N. Laroche
nans.laroche@tpac-ndt.com

E. Carcreff
ewen.carcreff@tpac-ndt.com

M. Rauch
matthieu.rauch@ec-nantes.fr

J.-Y. Hascoët
jean-yves.hascoet@ec-nantes.fr

[1] UMR CNRS 6183, Centrale Nantes/GeM, 1 rue de la Noë, 44321 Nantes, France

[2] Joint Laboratory of Marine Technology (JLMT) Centrale Nantes – Naval Group, Nantes, France

[3] UMR CNRS 6004, Centrale Nantes/LS2N, 1 rue de la Noë, 44321 Nantes, France

[4] The Phased Array Company (TPAC), 8 bis rue de la Garde, 44300 Nantes, France

SDH	Side drilled holes
SLM	Selective laser melting
TFM	Total focusing method
TOF	Time of flight
WAAM	Wire-arc additive manufacturing

Introduction

Direct energy deposition (DED) processes can be divided into two main technologies: laser metal deposition (LMD) and wire-arc additive manufacturing (WAAM). Usually, LMD is dedicated to thin walls and multi-graded components (Muller et al. 2013; Hascoët et al. 2011) whereas WAAM is used for structural and large-scale parts manufacturing (Kerninon et al. 2008). DED processes bring new opportunities for design and reduction of manufacturing cost, compared to standard processes like casting or machining. Nevertheless, the industrial implementation of DED processes is inhibited by the lack of structural health control. Regarding WAAM, final parts mechanical properties are currently limited by solidification defects, such as cracks and porosities, the latter being the major problem in case of aluminum alloys (Gu et al. 2014). The interested reader may refer to Williams' works for an in-depth discussion on defects in WAAM parts (Williams et al. 2016). Consequently, there is a real need to propose quality control techniques dedicated to DED-manufactured parts, in order to conclude on their integrity without damaging them. In this regard, ultrasonic non-destructive testing (NDT) techniques are promising means to inspect AM parts, either in an online or an offline manner. Additionally, to the measurement techniques, complementary approaches can predict the thermal behavior during the process and help to reduce the occurrence of thermal conditions conducive to defects formation. In this regard, numerical (Wei et al. 2017; Ogino et al. 2018; Xia et al. 2017) or analytical (Ning et al. 2019) approaches are particularly relevant.

In the literature, most ultrasonic NDT applications to AM metallic processes monitoring concern the selective laser melting (SLM) technology (Ning et al. 2019; Xu et al. 2017; Rieder et al. 2015; Carl 2015). Such NDT methods have to be adapted, particularly in terms of sensor precision and setup, to be suitable for defect characteristics encountered in DED (Gu et al. 2014; Williams et al. 2016). To the authors' best knowledge, no ultrasonic NDT application for LMD-manufactured parts has been published yet. As for WAAM, Obaton et al. (2018) and Lopez et al. (2018) identified several applicable ultrasonic NDT techniques for post-manufacturing inspections. They inspected aluminum alloy and mild-steel blocks and compared the NDT results with radiography and macrographic analysis. Recently, Lopez et al. (2017) tested several ultrasonic approaches on WAAM specimen with drilled defects using an ultrasonic wheel probe set up on a KUKA robot. Finally, some inspections guidelines have been given by Javadi et al. (2019), and particularly the idea to undertake in situ NDT measurements from below the substrate of the part being manufactured.

To date, the applications of ultrasonic NDT to WAAM samples focus on drilled defects only and do not consider actual defects induced by the process. Moreover, such studies are mainly discussing various techniques applicability and performances compared to other non-invasive control methods, and do not focus on the development of an accurate defect sizing method. Nevertheless, one of NDT applications main objectives is to quantitatively dimension flaws. That is why in the present paper, a specific phased array ultrasonic testing (PAUT) is presented and calibrated towards a quantitative sizing of the detected flaws. X-ray radiography is used to cross-check the PAUT predictions, yielding promising results to dimension flaw sizes from 0.6 to 1 mm. The UT method is applied to various specimens manufactured by WAAM, from a simple wall to an industrial blade of a propeller, in order to prove its relevance and control possibilities for industrial and complex parts. Finally, as this method is aimed at being integrated in a multi-sensor monitoring method for DED processes, currently developed in the GeM laboratory, some perspectives about in situ implementation are discussed, following Knezovic's guidelines (Javadi et al. 2019). This paper aims to be a proof of concept and opens the way to in situ ultrasonic control for metallic AM processes using PAUT.

Novel multi-sensor monitoring strategy for DED processes

This paper is part of current research dealing with a new multi-sensor monitoring method dedicated to DED processes (Knezovic and Dolsak 2018). This research follows previous papers dealing with closed-loop control of various manufacturing processes, such as machining (Chabot et al. 2019). The current study aims at developing a multi-physics monitoring methodology—as DED are complex processes with inter-dependent physical phenomena—with control strategies applicable to both powder and wire-fed DED processes.

The developed monitoring methodology is detailed in Fig. 1. As DED are complex processes with inter-dependent physical phenomena, it is necessary to consider multi-physics control strategies. At first, thermal and geometrical control loops were developed, as they are entangled phenomena both crucial for the correct manufacturing progress (Knezovic and Dolsak 2018). Even if it has been proved that controlling part geometry and temperature helps to control its integrity, such strategy gives limited means to

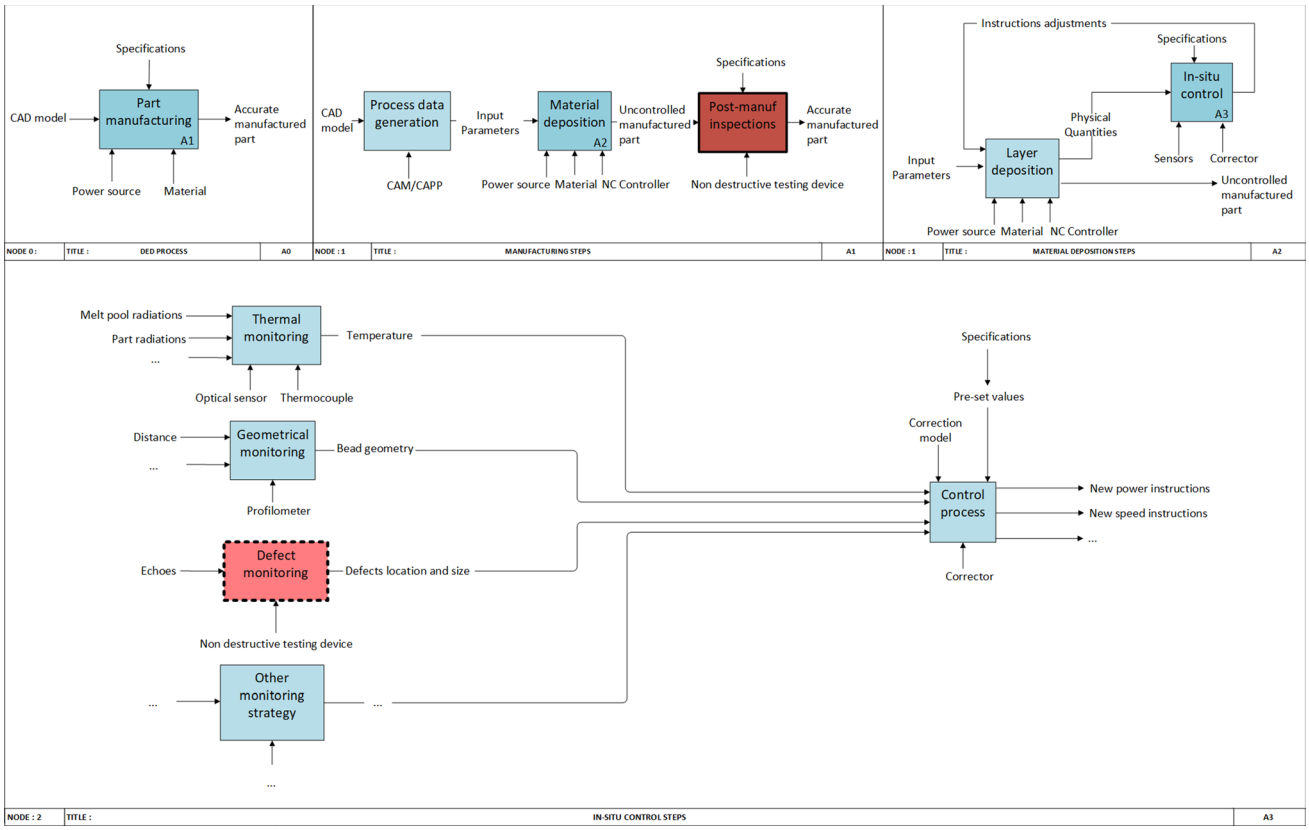

Fig. 1 Proposed methodology of multi-sensor monitoring for DED processes

assess the presence of defects—like porosities, gas inclusions, or local lack of fusion—formed during manufacturing as well as their size. That is why, it is relevant to provide a structural health monitoring strategy, in order to track defects formation during manufacturing, determine their cause in the manufacturing strategy, and save time and material by stopping the fabrication in case of bad structural health.

WAAM parts inspection using PAUT method

Materials and methods

WAAM parts manufacturing

Parts selected for the present work were manufactured in the multi-process unit of the GeM laboratory, illustrated in Fig. 2. The robotic unit includes a 6-axis KUKA robot suitable for hybrid—additive and subtractive—manufacturing, notably with high-speed machining, LMD and WAAM processes. In the present case, the robot was set up for the WAAM process with a gas metal arc welding (GMAW) torch. Parts were manufactured with a 5356-aluminum alloy

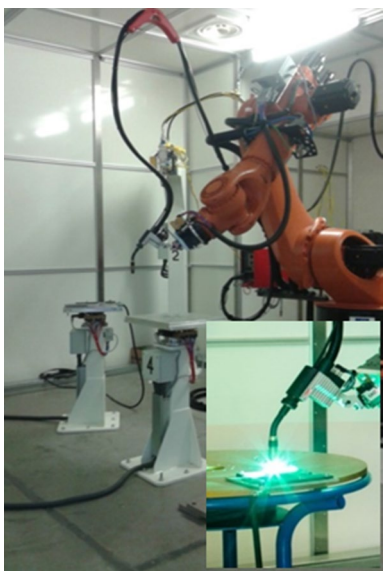

Fig. 2 Illustration of the multi-process robotic unit of the GeM laboratory

wire and typical process parameters for specimens considered in "Calibration of the PAUT method for defect sizing" and "Results and discussion" sections are given in Table 1.

Table 1 Process parameters for WAAM-manufactured specimens considered in "Calibration of the PAUT method for defect sizing" and "Results and discussion" sections

Power (W)	1100
Wire feed speed (mm/min)	8
Scanning speed (mm/min)	600

PAUT method

Ultrasonic testing (UT) is extensively used to control industrial parts (Poulhaon et al. 2014). Using multi-element probes, conventional phased array ultrasonic testing (PAUT) is a way to perform imaging which consists in applying a delay law in the hardware in order to focus the beam at specific points of the specimen under test. Other techniques consist in transmitting an unfocused beam in the material and to apply focusing in reception by post-processing the signal. In the PAUT family, the total focusing method (TFM) (Krautkramer and Krautkramer 1990) is a standard method to post-process the signal coming from all emitter-receiver pairs of an ultrasonic probe. For each pixel of a reconstruction grid, the time-of-flight (TOF) from the emitter to the pixel and from the pixel to the receiver is computed. Then, the intensity of the pixel is computed by summing and delaying the signals at the proper TOF. Such computations can be realized in parallel on graphic processing unit (GPU) in order to achieve real time imaging. This method provides a good resolution and signal to noise ratio, but it requires large computation capabilities. For more information on the TFM method and its application on AM-manufactured parts, the reader may refer to the comprehensive paper written by Xu et al. (2017). The plane wave imaging (PWI) (Holmes et al. 2005), widely used in the medical field, is similar to the TFM except that it uses plane waves transmitted simultaneously in the material with all elements. Overall, PWI has a lower resolution and signal to noise ratio than TFM, but it is more sensitive to small porosities and required fewer computing capabilities.

In this study, both TFM and PWI methods have been tested, alongside with several ultrasonic probes. With frame rates of 10 images per second and 100 images per second for TFM and PWI respectively, both methods are fast enough to allow real-time acquisition. Despite being slower than PWI, the TFM method has been selected due to its best image resolution.

Experimental PAUT setup

For PAUT, the probe design has to be adapted to the inspected material and the flaws to be detected (Montaldo et al. 2009). The frequency of the probe is linked to the wavelength of ultrasonic waves in the material and defines the minimum detectable defect size.

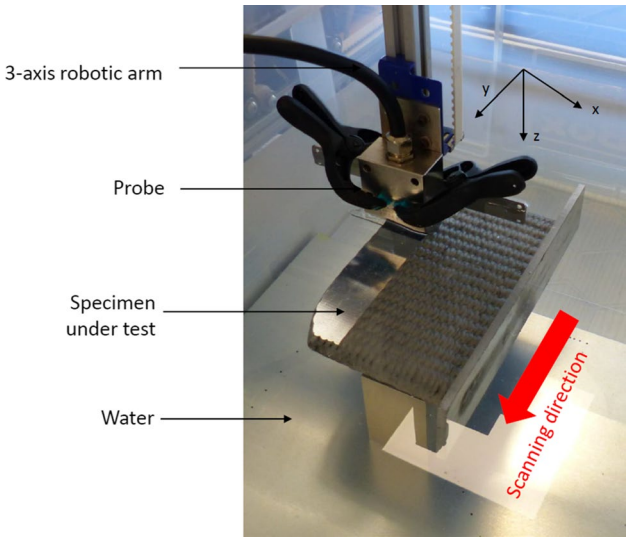

Fig. 3 Experimental setup for ultrasonic inspections of small parts

In this section, the selected ultrasonic device is the 128 channels Pioneer platform developed by TPAC (West Chester, Ohio, USA). A 10 MHz probe manufactured by Imasonic (Voray-sur-l'Ognon, FRANCE), with 80 elements activated out of 128 elements and an inter element space of 0.3 mm has been selected. This probe frequency gives a wavelength of 0.6 mm in WAAM samples; corresponding detection and sizing are possible for defects around 0.6 mm and larger. The exact same setup has been used for the next application cases presented in "WAAM parts inspection using PAUT method" section. All data have been acquired using the same digital and analogic gain of 10 dB and 45 dB respectively.

Ultrasonic inspections are performed with the sensor immersed in water. Two experimental setups have been used. The first experimental setup is pictured in Fig. 3. The part to be inspected is immersed in water and the probe is set on a 3-axis robotic arm. Due to the tank size, this setup is rather dedicated to small parts. For large parts, it is proposed to use a second setup, pictured in Fig. 4. For this setup, a water wedge is used. It can be assimilated to a bag filled with water and hermetically sealed on the transducers of the probe, in order to locally replicate the water coupling. These two setups reduce the dead zone below the surface created by the impedance change between the coupling and the media and enable to perform inspections of parts with complex surfaces.

For both presented setups, 3D scans of the specimen under test are performed by moving the probe. Results are presented in three 2D graphs, as illustrated in Fig. 5. The three graphs are called Bscan, Cscan and Dscan, corresponding to the X–Z, X–Y, and Y–Z planes respectively. Each image is a reconstruction of the ultrasonic echoes measured

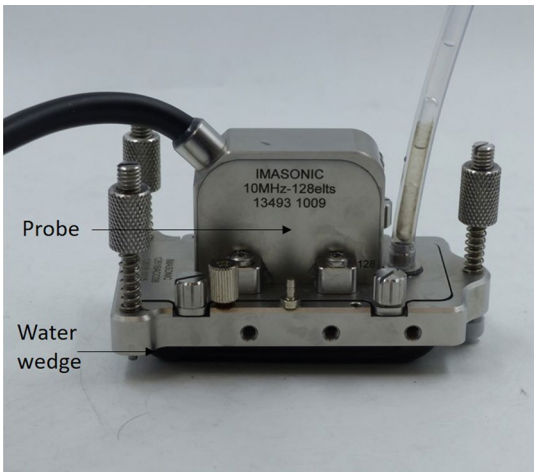

Fig. 4 Experimental setup for ultrasonic inspections of large parts

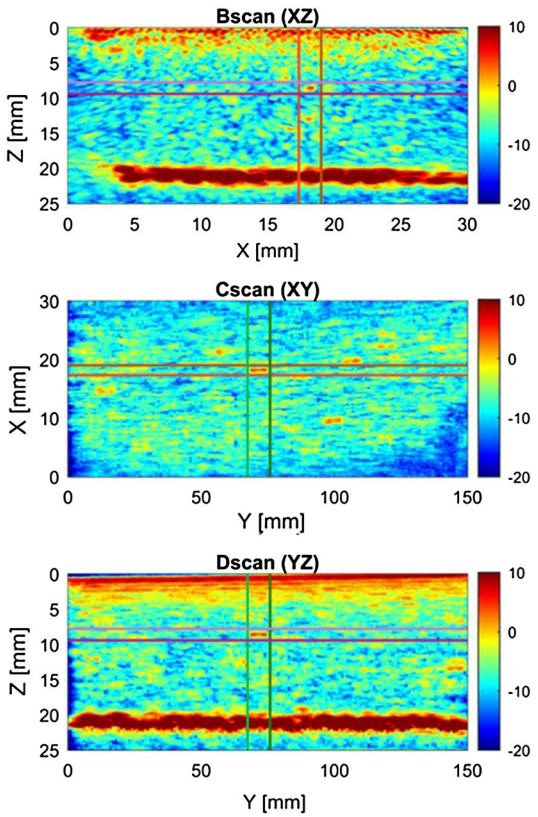

Fig. 5 Example of ultrasonic 3D results, scale in dB

by the probe transducers. The amplitude of each voxel is computed using the vertical envelope process in order to get a positive image without echo oscillations. Then, the volume is computed in dB and the acquisition gains are removed from the image to get a standard value independent from the acquisition settings. To compute the intensity of a pixel in a 2D image from the 3D volume, the maximum value along the third dimension is considered.

In Fig. 5, both Dscan and Bscan show two strong echoed lines, at Z locations 0 mm and 20 mm, corresponding to the top and bottom surfaces of the specimen under test. Several reflectors are detected on the images; they are particularly visible on the Cscan.

In this study, the inspections of WAAM specimens showed that most detected reflectors were nearly spherical, and thus can be assimilated to actual porosities. Such porosities may either be a lack of deposited material induced by insufficient overlap between beads, or inclusions of protection gas between layers created during deposition.

Calibration of the PAUT method for defect sizing

The aim of this section is to link the size of calibrated defects to the results of the PAUT scans. The calibration is performed on an aluminum alloy 5356 WAAM-manufactured multi-layered block, machined to the dimensions of 140 mm, 60 mm and 20 mm. Three sets of four holes, with diameters ranging from Ø0.6 mm to Ø1.2 mm, were drilled at three different depths, namely 10 mm, 30 mm and 50 mm from the top surface, as shown in Fig. 6a, b tails how the calibration block has been positioned in the immersion setup, the X axis being the scanning direction.

As the calibration block is inspected perpendicularly to the hole direction, side-drilled holes (SDH) are observed. Preliminary inspections have shown that the defect intensity—or number of reflected echoes—depends on its depth and lateral position in regard with the probe, its diameter and its shape but also the probe characteristics and the imaging methods. Such results are corroborated by Felice et al. in their review (Felice and Fan 2018). Consequently, in the present paper, the SDH intensity is linked to its diameter and distance to the probe centre. To the authors best knowledge, no analytical model computing the flaw intensity depending on such parameters has been developed yet. That is why, as first approach, a Gaussian process has been chosen to evaluate margins of error depending on the experimental data. For more information about the Gaussian process, the reader may refer to Rasmussen and Williams' book (Rasmussen and Williams 2006).

The calibration method has been implemented on the 10-mm depth set of defects of the WAAM calibration block. Figure 7 gives a typical ultrasonic image of the four 10-mm depth SDH. Four different parallel scans have been performed to estimate the method repeatability. For each scan, a data set is acquired every 0.5 mm over a range of 32 mm for a total of 64 data sets per scan. An ultrasonic image is computed for each data set, and the intensity and distance to the center of the probe are computed for each detected flaw. These values are added to the corresponding calibration

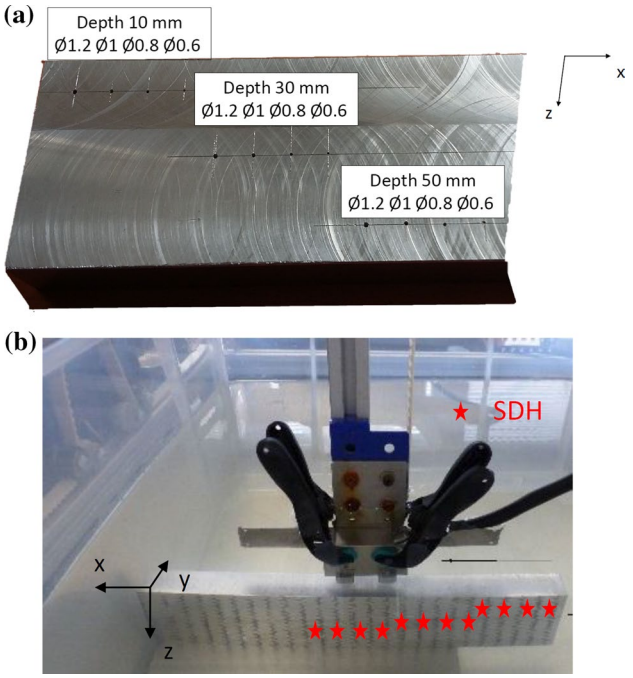

Fig. 6 **a** Aluminum alloy block designed for the UT calibration. **b** Experimental setup for calibration inspections

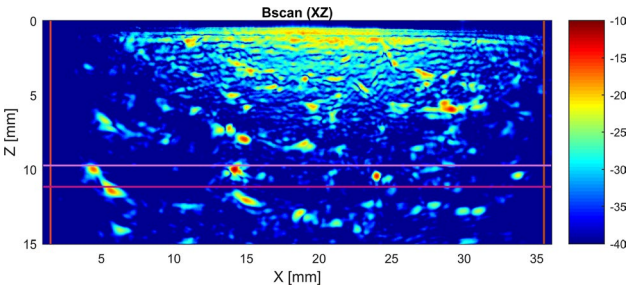

Fig. 7 Ultrasonic image of the 10 mm-depth SDH of the calibration block, scale in dB

abacus presented in Fig. 8. Thus, more than 250 ultrasonic images have been studied in this experiment.

In Fig. 8, each calibration curve corresponds to a specific defect diameter. For each defect size, points represent the intensities of the corresponding SDH measured in several ultrasonic images. The plain lines show the mean of the posterior Gaussian process while the colored region is a 90% confidence interval which depends on the variability of the samples and the number of samples per region. In Fig. 8, the amplitude is nearly constant around the center of the probe, as it corresponds to an area where all the probe elements are contributing to the defect detection. Then, the amplitude decreases as the distance to the probe center rises. The intensity also rises with the size of the flaws, possibly allowing the determination of the flaw size from the PAUT

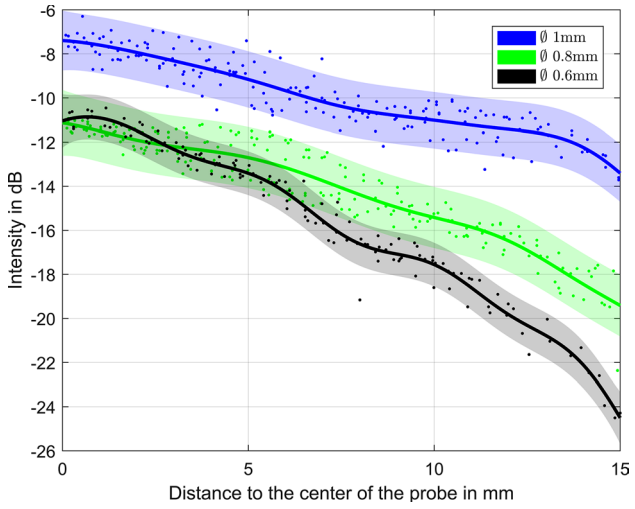

Fig. 8 Calibration abacus for the selected configuration

scans. Except for a small area where the curves of 0.6 and 0.8 mm overlap, the three sizes of flaws are quite distinct.

Considering the present detection range, the selected PAUT method is promising for in situ structural integrity control, as the process could be stop during manufacturing in case of large defects detected, which would help to save both material and manufacturing time. A more comprehensive calibration study would broaden the detection range of the method. For smaller metallurgical pores, which affect the mechanical properties of the part, numerical approaches may also be used to optimize deposition conditions and limit their apparition in the melt pool (Xia et al. 2017).

Results and discussion

Application on an aluminum alloy block: confrontation of the defect sizing method to X-ray radiography

In this section, X-ray imaging is used to cross-check porosity detection with PAUT. At first, ultrasonic inspections are performed on a multi-layer aluminum alloy wall. The dimensions are 155-mm high, 100-mm long and 20-mm wide. One surface has been partially machined in order to perform the ultrasonic inspection, as shown in Fig. 9.

Digital radiography testing (RT) has been performed on the multi-layered wall, and two porosities have been selected to assess the calibration of the PAUT method and prove its potential. For each porosity, sizing results are detailed in Table 2. Figures 10 and 11 show the ultrasonic and X-ray inspections of defect #1 respectively. Similarly, Figs. 12 and 13 show the ultrasonic and X-ray inspections of defect #2. The first porosity has been detected in three different acquisitions, the mean and standard deviation of the three values being displayed in Table 1.

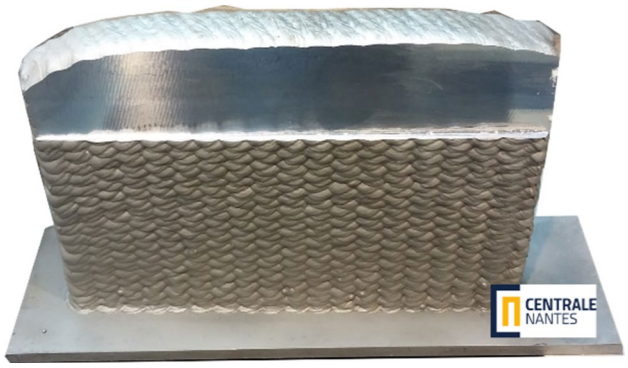

Fig. 9 WAAM multi-layered aluminum alloy wall selected for UT inspections

Table 2 Sizing of porosities #1 and #2 from both UT and RT

	Porosity #1	Porosity #2
Amplitude (dB)	$-23.50^{\pm 1.70}$	−16.24
Distance from probe center (mm)	$9.57^{\pm 1.40}$	1.10
Depth from surface (mm)	11.75	4.80
Estimated size from PAUT (mm)	< 0.6	< 0.6
Estimated size from RT (mm)	0.69	0.88

In the PAUT scans pictured in Fig. 10, porosity #1 has been measured at 9.57 mm from the center of the probe with an amplitude of − 23.50 dB. According to the calibration abacus—see Fig. 8—, the corresponding size is slightly smaller than 0.6 mm. The X-ray tomography estimated the porosity size at 0.69 mm, as shown in Fig. 11. Similarly, in the PAUT scans pictured in Fig. 12, porosity #2 has been measured at 1.10 mm from the center of the probe with an amplitude of − 16.24 dB. According to the calibration abacus—see Fig. 8—, the corresponding size is significantly smaller than 0.6 mm. RT estimated the porosity size at 0.88 mm, as shown in Fig. 13.

For both selected porosities, the defect size has been under-estimated by the PAUT method compared to X-ray radiography. This is linked to the fact that an SDH is more echogenic than the detected porosities. A calibration step on real defects—possibly non-spherical and non-piercing defects like porosities—usually encountered in AM parts is expected to improve significantly the sizing results. In this way, micro-computed tomography or other NDT methods can be taken as a reference in order to size the defects with more precision. A dedicated numerical method from ultrasonic images acquired on a calibration block is also effective to quantitatively infer the defect geometry.

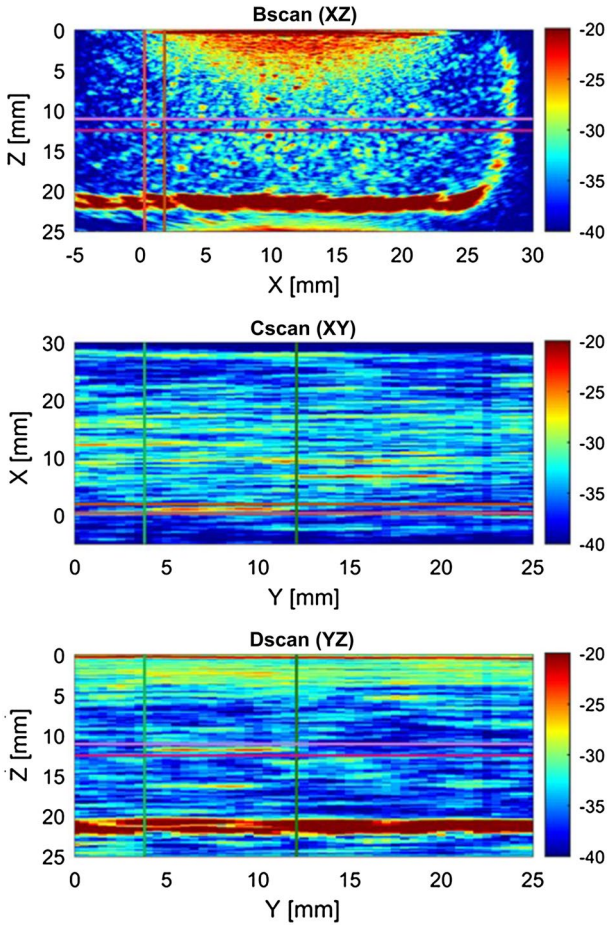

Fig. 10 PAUT inspection of porosity #1, scale in dB

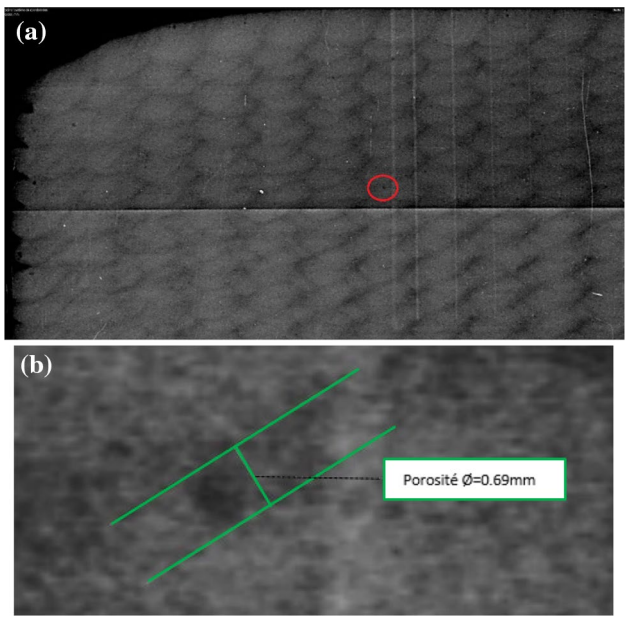

Fig. 11 Radiography of the WAAM specimen. **a** Global view near porosity #1. **b** Sizing of porosity #1

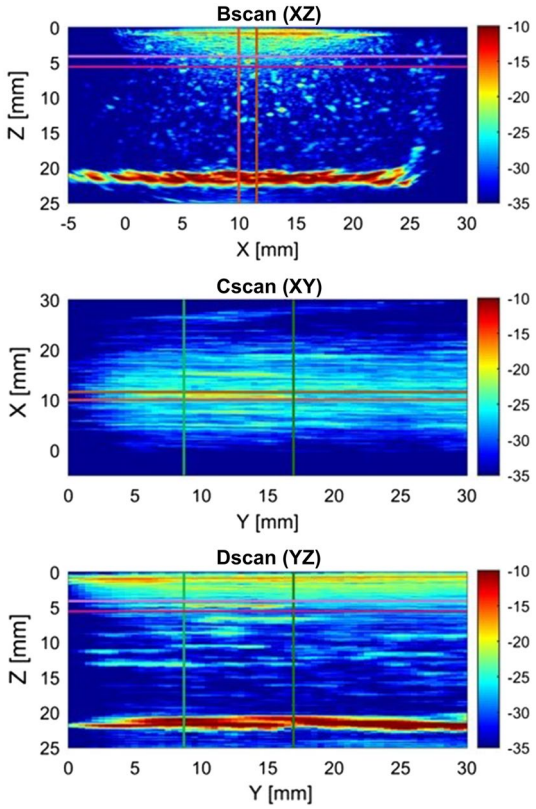

Fig. 12 PAUT inspection of porosity #2, scale in dB

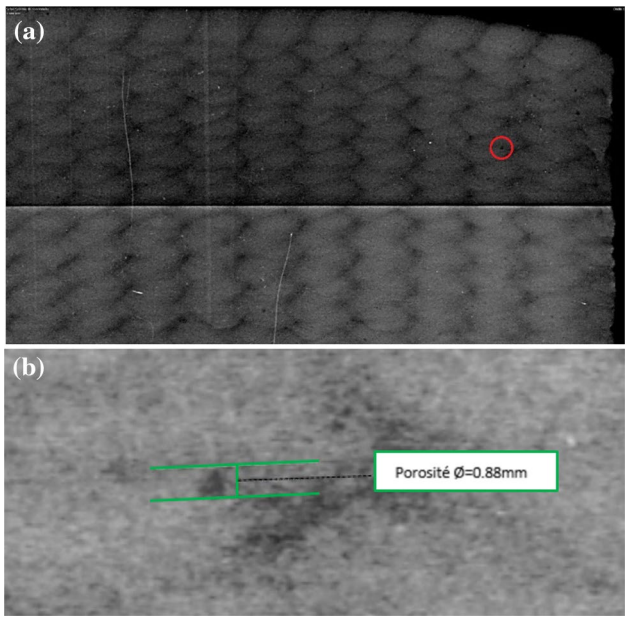

Fig. 13 Radiography of the WAAM specimen. **a** Global view near porosity #2. **b** Sizing of porosity #2

Fig. 14 WAAM-manufactured propeller

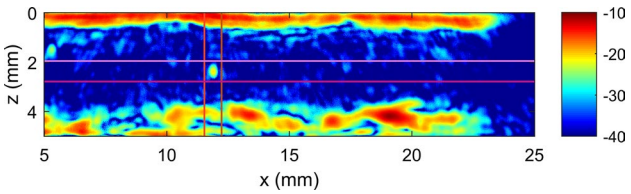

Fig. 15 Example of ultrasonic image from the inspection of the WAAM-manufactured propeller, scale in dB

Application on a WAAM-manufactured industrial propeller

The present section illustrates an applicable scenario of the PAUT method on a large-scaled and complex-shaped part. This applicable scenario gives promising perspectives towards a comprehensive structural integrity control of real and industrial components (Fig. 14).

A hollow-blade aluminum alloy propeller has been selected for the present inspections, as it is representative of a large range of structures encountered in the aeronautical and naval fields. The propeller is pictured in Fig. 15: it has a 1050-mm diameter, and its blades have been manufactured by WAAM and machined after deposition. One blade of the propeller has been inspected. The inspections were conducted using the water wedge system, illustrated in Fig. 4, as the propeller size was not suitable for the immersion setup. The PAUT probe was positioned perpendicularly to the direction of the deposited layers. An adaptive algorithm that detects the surface and computes the image from a single data sample was applied (Le Jeune et al. 2015). An example of ultrasonic images is shown in Fig. 15.

In Fig. 15, it can be noticed that the inspected area is only 3-mm deep, which corresponds to one side of the hollow blade. The bottom echo is noisier than the top one because

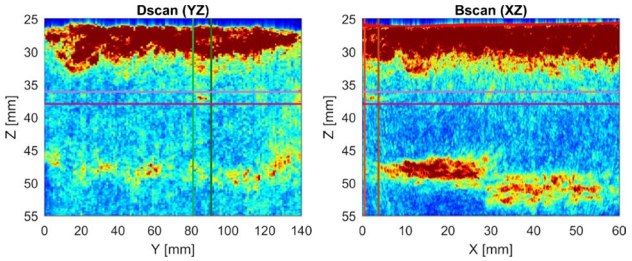

Fig. 16 Inspection from a raw AM-manufactured surface

of their surface properties, namely machined at the top and left raw from AM deposition at the bottom. Figure 15 shows one nearly-spherical defect, located around 2 mm from the middle of the probe and with an amplitude of − 22.75 dB. According to the calibration abacus—see Fig. 8—this defect is dimensioned significantly smaller than 0.6 mm.

Perspectives for in situ applications

Previous section showed that the PAUT method is suitable for post-manufacturing inspections on various WAAM parts. In this section, the in situ applicability of the method is studied towards a future implementation. More particularly, two challenges are discussed: first, performing scan on rough surfaces, in view of inspecting the part between deposition steps, and stop manufacturing before the end in case of bad structural health; second, inspection from below the substrate, following Knezovic's guidelines towards online acquisitions (Knezovic and Dolsak 2018).

First, Fig. 16 provides some results for PAUT inspections from a surface left raw from WAAM deposition. The ultrasonic images in Fig. 16 concern the multi-layered block from "Material and methods" section, inspected from the AM-manufactured side, with a 5 MHz probe.

Comparing the ultrasonic images of Figs. 5 and 16, it can be noted that the data are noisier, due to the irregularities of the AM-manufactured surface. This noisiness is particularly visible on the Bscan of Fig. 16, with a top echo being around 5-mm large, compared to less than 1 mm in Fig. 5. The machined and raw surfaces can be noticed at the bottom-echo of the Bscan, respectively for X ranging from 0 to 30 mm and 30 to 60 mm. Despite the increased noise, a porosity is detected at approximately X = 5 mm, Y = 85 mm and Z = 37 mm. This defect has also been found in the radiography. Consequently, the selected PAUT method could be implemented on WAAM components without needing post-manufacturing surface rectifications. However, the surface irregularities have to be smaller than the wavelength, thus we recommend using a lower frequency for an inspection from a raw surface. As a consequence, larger defects may be detected in this in situ configuration, compared to the 0.6–1 mm range previously reported for inspections on a machined surface.

Second, measurements from below the substrate have been tested with a 5 MHz probe, following Knezovic's guidelines (Knezovic and Dolsak 2018). First results are provided in Fig. 17: as illustrated in Fig. 17b, c, defects can be detected from below the substrate. These measurements perspectives, added with the processing speed of the ultrasonic images and the compact design of the equipment, make the measurement technique compatible with the environment method and promising for in situ applications. Specific algorithms for images analysis and defects classification

Table 3 Process parameters for the LMD-manufactured specimen

Power (W)	1300
Powder flow rate (g/min)	20
Scanning speed (mm/min)	1900

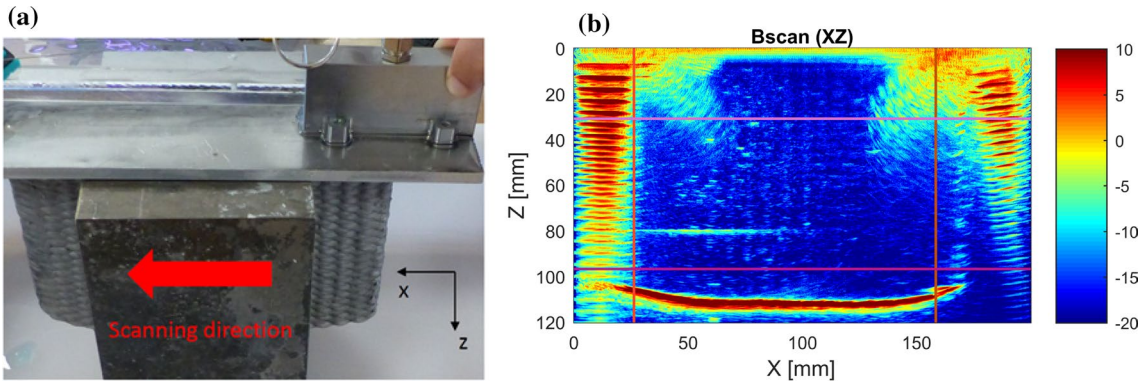

Fig. 17 Ultrasonic inspection of the multi-layered aluminum alloy block from below the substrate. **a** Experimental setup, **b** Bscan graph of the global part, scale in dB

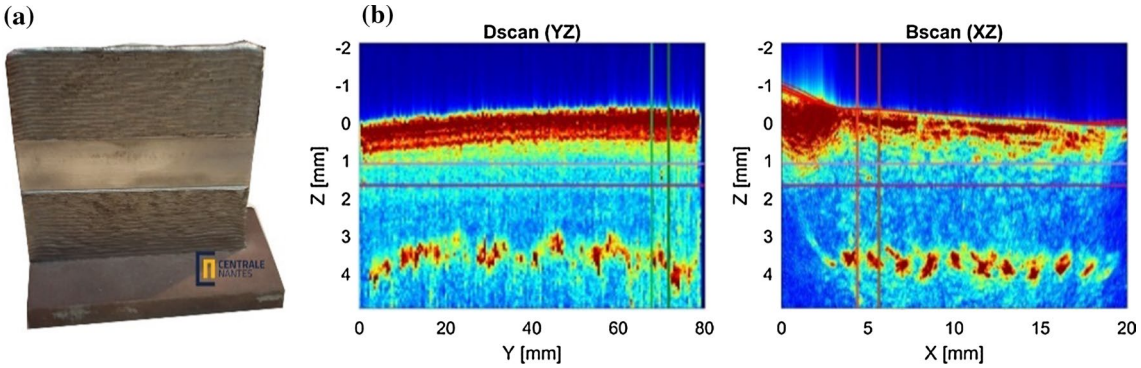

Fig. 18 Proof of NDT method adaptability to LMD. **a** LMD-manufactured specimen. **b** Corresponding ultrasonic inspections

are expected to improve the inspection results (Kwon et al. 2018; Panda et al. 2019).

Method applicability on LMD components

This section opens the way to similar PAUT inspections to LMD parts. As the characteristic defect size is much smaller in LMD. It requires the use of a probe with a higher frequency.

In this study, a 18.5 MHz probe with 128 elements and 0.26 mm hatch space has been selected. The specimen is a stainless-steel LMD-manufactured wall, with process parameters detailed in Table 3. One particular defect at location X = 5 mm, Y = 80 mm and Z = 9 mm, has been detected in the ultrasonic images from Fig. 18. The calibration study proposed in "Calibration of the PAUT method for defect sizing" section could be conducted on such kind of ultrasonic images from LMD parts inspection in order to confirm the versatility of the presented NDT method.

Conclusion

This work is part of current developments at the GeM laboratory to develop a multi-physics monitoring methodology for DED processes. In this paper, a promising ultrasonic NDT method has been presented to control DED-manufactured components.

A particular attention has been devoted to the method calibration, towards accurate sizing of the detected reflectors. The PAUT sizing predictions were cross-checked with X-ray radiography which enabled to conclude on the method ability to detect defects whose size are between 0.6 mm to 1 mm for aluminum alloy components. The applicability of the inspection procedure has been illustrated on various scenarios, from blocks to industrial and large-scale components. The presented inspection procedure can be similarly led on LMD parts, provided the use of a probe with a higher frequency. Perspectives concerning an in situ application of the PAUT method during DED manufacturing have been discussed. The reliable defect sizing step, added with the equipment compact design, processing speed and ability to perform measurements on a rough surface, make the proposed PAUT method promising for in situ control of a certain range of components. Furthermore, Knezovic and Dolsak (2018) have proposed several solutions for the sensor integration in the manufacturing environment to achieve online acquisitions and real-time structural health control.

However, this study is a proof of concept, and many challenges are still to be faced—comprehensive calibration of the method, further capabilities assessment and enhanced images processing—to develop a robust online and offline control for metallic AM parts.

References

Carl, V. (2015). Monitoring system for the quality assessment of additive manufacturing. *AIP Conference Proceedings, 1650,* 171. https://doi.org/10.1063/1.4914607.

Chabot, A., Rauch, M., & Hascoët, J.-Y. (2019). Towards a multi-sensor monitoring methodology for AM metallic processes. *Journal Welding in the World*. https://doi.org/10.1007/s40194-019-00705-4.

Felice, M. V., & Fan, Z. (2018). Sizing of flaws using ultrasonic bulk wave testing: A review. *Ultrasonics, 88,* 26–42.

Gu, J., Cong, B., Ding, J., Williams, S. W., & Zhai, Y. (2014). Wire + arc additive manufacturing of aluminium. In *Solid freeform fabrication symposium*, Austin, Texas (pp. 451–458).

Hascoët, J.-Y., Muller, P., & Mognol, P. (2011). Manufacturing of complex parts with continuous functionally graded materials (FGM). In *Solid freefrom fabrication symposium* (pp. 557–569).

Holmes, C., Drinkwater, B., & Wilcox, P. (2005). Post-processing of the full matrix of ultrasonic transmit–receive array data for non-destructive evaluation. *NDT&E International, 38*(8), 701–711.

Javadi, Y., Macleod, C. N., Pierce, S. G., Gachagan, A., Kerr, W., Ding, J., et al. (2019). Ultrasonic phased array inspection of wire + arc

additive manufacture samples using conventional and total focusing method imaging approaches. *Insight, 61,* 298–306.

Kerninon, J., Mognol, P., Hascoet, J.-Y., & Legonidec, C. (2008). Effect of path strategies on metallic parts manufactured by additive process. In *Solid freeform fabrication symposium* (pp. 352–361).

Knezovic, N., & Dolsak, B. (2018). In-process non-destructive ultrasonic testing application during wire plus arc additive manufacturing. *Advances in Production Engineering & Management, 13*(2), 158–168.

Krautkramer, J., & Krautkramer, H. (1990). *Ultrasonic testing of materials*. Berlin: Springer.

Kwon, O., Kim, H. G., Ham, M. J., Kim, W., Kim, G. H., Cho, J. H., Kim, N. I., & Kim, K. (2018). A deep neural network for classification of melt-pool images in metal additive manufacturing. *Journal of Intelligent Manufacturing*, 1–12.

Le Jeune, L., Robert, S., Membre, A., & Prada, C. (2015). Adaptative ultrasonic imaging with the total focusing method for inspection of complex components immersed in water. In *41st annual review of progress in quantitative non-destructive evaluation*, Boise, Idaho (Vol. 34, pp. 1037–1046).

Lopez, A., Bacelar, I., Pires, I., Santos, T., & Quintino, L. (2017). Mapping of non-destructive techniques for inspection of wire + arc additive manufacturing. In *Proceedings of 7th international conference on mechanics and materials in designing,* Portugal (pp. 1829–1844).

Lopez, A., Bacelar, R., Pires, I., Santos, T. G., Sousa, J. P., & Quitino, L. (2018). Non-destructing testing application of radiography and ultrasound for wire and arc additive manufacturing. *Additive Manufacturing, 21,* 298–306.

Montaldo, G., Tanter, M., Bercoff, J., Benech, N., & Fink, M. (2009). Coherent plane-wave compounding for very high frame rate ultrasonography and transient elastography. *IEEE Transactions on Ultrasonics, Ferroelectrics, and Frequency Control, 56*(3), 489–506.

Muller, P., Mognol, P., & Hascoet, J.-Y. (2013). Modeling and control of a direct laser powder deposition process for functionally graded materials (FGM) parts manufacturing. *Journal of Material Processing Technology, 213*(5), 685–692.

Ning, J., Sievers, D. E., Garmestani, H., & Liang, S. Y. (2019). Analytical modeling of in-process temperature in powder bed additive manufacturing considering laser power absorption, latent heat, scanning strategy, and powder packing. *Materials, 12*(5), 808.

Obaton, A.-F., Butsch, B., McDonough, S., Carcreff, E., Laroche, N., Gaillard, Y., Tarr, J. B., Bouvet, P., Cruz, R., & Donmez, A. (2018). Evaluation of non-destructive volumetric testing methods for additively manufactured parts. In *ASTM symposium on structural integrity of additive manufactured parts*, Washington, DC.

Ogino, Y., Asai, S., & Hirata, Y. (2018). Numerical simulation of WAAM process by a GMAW weld pool model. *Welding in the World, 62*(2), 393–401.

Panda, B., Shankhwar, K., Garg, A., & Savalani, M. M. (2019). Evaluation of genetic programming-based models for simulating bead dimensions in wire and arc additive manufacturing. *Journal of Intelligent Manufacturing, 30*(2), 809–820.

Poulhaon, F., Rauch, M., Leygue, A., Hascoet, J.-Y., & Chinesta, F. (2014). Online prediction of machining distortion of aeronautical parts caused by re-equilibration of residual stresses. *Key Engineering Materials, 611–612,* 1327–1335.

Rasmussen, C. E., & Williams, C. K. I. (2006). *Gaussian processes for machine learning*. Cambridge, MA: MIT Press.

Rieder, H., Dillhofer, A., & Spies, M. (2015). Ultrasonic online monitoring of additive manufacturing processes based on selective laser melting. *Review of Progress in Quantitative Nondestructive and Evaluation, 1650*(1), 84–191.

Wei, P., Wei, Z., Chen, Z., He, Y., & Du, J. (2017). Thermal behavior in single track during selective laser melting of AlSi10Mg powder. *Applied Physics A, 123*(9), 604.

Williams, S. W., Martina, F., Addison, A. C., Ding, J., Pardal, G., & Colegrove, P. (2016). Wire + arc additive manufacturing. *Materials Science and Technology, 32*(7), 641–647.

Xia, M., Gu, D., Yu, G., Dai, D., Chen, H., & Shi, Q. (2017). Porosity evolution and its thermodynamic mechanism of randomly packed powder-bed during selective laser melting of Inconel 718 alloy. *International Journal of Machine Tools and Manufacture, 116,* 96–106.

Xu, N., Shi, Y. W., He, F. C., & Yang, P. H. (2017). Ultrasonic array inspection for additive manufacturing components using full matrix capture. In *15th Asia Pacific conference for non-destructive testing,* Singapore.